

1 **Title: Impaired immune signaling and changes in the lung microbiome precede secondary**  
2 **bacterial pneumonia in COVID-19**

3

4 **Authors:**

5 †Alexandra Tsitsiklis<sup>1</sup>, †Beth Shoshana Zha<sup>2</sup>, †Ashley Byrne<sup>3</sup>, †Catherine Devoe<sup>1</sup>, #Sophia Levan<sup>4</sup>,  
6 #Elze Rackaityte<sup>5</sup>, Sara Sunshine<sup>5</sup>, Eran Mick<sup>1,2,3</sup>, Rajani Ghale<sup>1,2</sup>, Alejandra Jauregui<sup>2</sup>, Aartik  
7 Sarma<sup>2</sup>, Norma Neff<sup>3</sup>, Paula Hayakawa Serpa<sup>1</sup>, Thomas J. Deiss<sup>2</sup>, Amy Kistler<sup>3</sup>, Sidney Carrillo<sup>2</sup>,  
8 K. Mark Ansel<sup>6,7</sup>, Aleksandra Leligdowicz<sup>2</sup>, Stephanie Christenson<sup>2</sup>, Norman Jones<sup>8</sup>, Bing Wu<sup>9</sup>,  
9 Spyros Darmanis<sup>9</sup>, Michael A. Matthay<sup>2</sup>, Susan V. Lynch<sup>10,11</sup>, Joseph L. DeRisi<sup>3,5</sup>, COMET  
10 Consortium+, Carolyn M. Hendrickson<sup>2</sup>, Kirsten N. Kangelaris<sup>4</sup>, Matthew F. Krummel<sup>12</sup>, Prescott  
11 G. Woodruff<sup>2,7</sup>, David J. Erle<sup>4,13,14</sup>, Oren Rosenberg<sup>1</sup>, Carolyn S. Calfee<sup>2</sup>, \*Charles R. Langelier<sup>1,3</sup>

12

13 †#equal contributions

14

15 **Affiliations:**

16 <sup>1</sup>Department of Medicine, Division of Infectious Diseases, University of California San Francisco,  
17 San Francisco, CA, USA

18 <sup>2</sup>Department of Medicine, Division of Pulmonary, Critical Care, Allergy and Sleep Medicine,  
19 University of California San Francisco, San Francisco, CA, USA

20 <sup>3</sup>Chan Zuckerberg Biohub, San Francisco, CA, USA

21 <sup>4</sup>Department of Medicine, University of California San Francisco, San Francisco, CA, USA

22 <sup>5</sup>Department of Biochemistry and Biophysics, University of California San Francisco, San  
23 Francisco, CA, USA

24 <sup>6</sup>Department of Microbiology and Immunology, University of California, San Francisco, CA, USA

25 <sup>7</sup> Sandler Asthma Basic Research Center, University of California, San Francisco, CA, USA

26 <sup>8</sup>Department of Experimental Medicine, University of California, San Francisco, CA, USA

27 <sup>9</sup> Genentech, Inc. San Francisco, CA, USA.

28 <sup>10</sup> Department of Gastroenterology, University of California, San Francisco, CA, USA

29 <sup>11</sup> Benioff Center for Microbiome Medicine, University of California, San Francisco, CA, USA

30 <sup>12</sup> Department of Pathology, University of California, San Francisco, CA, USA

31 <sup>13</sup> Lung Biology Center, University of California, San Francisco, CA, USA

32 <sup>14</sup> UCSF CoLabs, University of California, San Francisco, CA, USA

33 <sup>+</sup>COMET (COVID-19 Multiphenotyping for Effective Therapies) Consortium members are listed  
34 in the Supplementary Appendix.

35

36

37 \*Corresponding author

38 Email: [chaz.langelier@ucsf.edu](mailto:chaz.langelier@ucsf.edu)

39

40 **Keywords:** COVID-19, SARS-CoV-2, secondary bacterial pneumonia, VAP, metagenomics,

41 scRNA-seq

42

43 **Abstract**

44           Secondary bacterial infections, including ventilator-associated pneumonia (VAP), lead to  
45 worse clinical outcomes and increased mortality following viral respiratory infections including in  
46 patients with coronavirus disease 2019 (COVID-19). Using a combination of tracheal aspirate  
47 bulk and single-cell RNA sequencing (scRNA-seq) we assessed lower respiratory tract immune  
48 responses and microbiome dynamics in 28 COVID-19 patients, 15 of whom developed VAP, and  
49 eight critically ill uninfected controls. Two days before VAP onset we observed a transcriptional  
50 signature of bacterial infection. Two weeks prior to VAP onset, following intubation, we observed  
51 a striking impairment in immune signaling in COVID-19 patients who developed VAP. Longitudinal  
52 metatranscriptomic analysis revealed disruption of lung microbiome community composition in  
53 patients with VAP, providing a connection between dysregulated immune signaling and outgrowth  
54 of opportunistic pathogens. These findings suggest that COVID-19 patients who develop VAP  
55 have impaired antibacterial immune defense detectable weeks before secondary infection onset.

56 **Introduction**

57           Secondary bacterial pneumonia results in significant morbidity and mortality in patients  
58 with viral lower respiratory tract infections (LRTI)<sup>1</sup>. This problem was evident in the 1918 influenza  
59 pandemic during which the majority of deaths were ultimately attributed to secondary bacterial  
60 pneumonia<sup>2</sup>. SARS-CoV-2 infection, like influenza, confers an increased risk of late onset  
61 secondary bacterial infection, often manifesting as ventilator-associated pneumonia (VAP)<sup>3</sup>.  
62 Marked heterogeneity exists with respect to the risk of VAP in patients with coronavirus disease  
63 2019 (COVID-19), with incidence ranging from 12-87% between published cohort studies<sup>4-7</sup>.

64           The mechanisms underlying VAP susceptibility in COVID-19 remain unknown, and no  
65 biomarkers yet exist to inform risk of VAP at the time of intubation. Animal models of influenza  
66 may provide some insight, suggesting a role for interferon-mediated suppression of cytokines  
67 essential for bacterial defense, including neutrophil recruitment, antimicrobial peptide production  
68 and the Th17 response<sup>8-10</sup>. Few human immunoprofiling studies have been conducted in VAP  
69 however, and none have been reported in a prospective cohort of COVID-19 patients.

70           Lower respiratory infections represent a dynamic relationship between pathogen, host  
71 response and the lung microbiome<sup>11</sup>. Despite their interconnected roles, no studies to date have  
72 simultaneously profiled host immune responses and lung microbiome dynamics in the context of  
73 VAP. For instance, while prior work has described lung microbiome disruption in patients with  
74 VAP<sup>11,12</sup>, the question of whether host immune responses following viral infection may contribute  
75 to this dysbiosis, leading to subsequent infection, remains unanswered.

76           Given the marked heterogeneity in VAP incidence among patients with COVID-19<sup>4-7</sup>, as  
77 well as gaps in mechanistic understanding of secondary bacterial pneumonia, we sought to  
78 assess the molecular determinants of VAP in the setting of SARS-CoV-2 infection. We employed  
79 a systems biology approach involving immunoprofiling the host transcriptional response and  
80 simultaneously assessing lung microbiome dynamics, using a combination of bulk and single cell  
81 RNA sequencing and extensive clinical phenotyping. We observed a striking impairment in

82 antibacterial immune signaling at the time of intubation, that correlated with disruption of the lung  
83 microbiome, weeks before the onset of VAP.

84

## 85 **Results**

86 We conducted a prospective case-control study of adults requiring mechanical ventilation  
87 for COVID-19 or for illnesses other than pneumonia. Of 84 patients with COVID-19 initially  
88 enrolled, tracheal aspirate (TA) specimens from 28 patients met inclusion criteria for analysis  
89 (**Methods, Figure 1**). In addition, eight critically ill patients from a second cohort (Study 2,  
90 **Methods**) were included as controls. Patients were enrolled at one tertiary care hospital and one  
91 safety net hospital in San Francisco, California under research protocols approved by the  
92 University of California San Francisco Institutional Review Board (**Methods**). We collected TA  
93 periodically following intubation and performed bulk and scRNA-seq (**Methods**).

94 Patients with VAP were adjudicated using the United States Centers for Disease Control  
95 (CDC) definition<sup>13</sup>, including a requirement for a positive bacterial TA culture (N=10). Patients who  
96 met CDC VAP criteria but had negative bacterial TA cultures were only included in a secondary  
97 analysis (N=5). We defined onset of VAP as the first day a patient developed any of the criteria  
98 used to meet the definition, in accordance with CDC guidance. Patients who did not meet the  
99 CDC-NHSN criteria for VAP, and for whom there was no sustained clinical suspicion for bacterial  
100 pneumonia during the admission, were adjudicated as No-VAP (N=13).

101 We compared lower respiratory tract host transcriptional responses between the VAP and  
102 No-VAP groups at two time points. “Early” time point TA samples were collected a median of two  
103 days post-intubation and 17 days before VAP onset (bulk RNA-seq analysis) or nine days before  
104 VAP onset (scRNA-seq). “Late” time point samples were collected a median of two days before  
105 VAP onset for both bulk and scRNA-seq analyses and compared against samples collected from  
106 No-VAP patients at similar timepoints post-intubation (**Figure 1, Table S1, Table S2**). We  
107 additionally evaluated eight intubated patients with non-pneumonia illnesses as controls at the

108 “early” time-point. There were no significant differences between groups with respect to age,  
109 gender, race or ethnicity (**Table S1, S2**). In addition, there were no differences between groups  
110 with respect to in-hospital receipt of any immunosuppressant or antibiotics prior to sample  
111 collection (**Table S3**).

112

### 113 **COVID-19 VAP is associated with a transcriptional signature of bacterial infection two days** 114 **before VAP onset**

115 We began by assessing the lower respiratory host transcriptional response two days  
116 preceding VAP onset in COVID-19 patients. Differential gene expression analysis was carried out  
117 on TA bulk RNA-seq data from five patients who developed VAP (samples collected a median of  
118 two days before VAP onset) and eight patients who did not develop VAP collected within a similar  
119 time frame after intubation (**Table S1**). We identified 436 differentially expressed genes at a False  
120 Discovery Rate (FDR) < 0.1 (**Figure 2A**) and performed gene set enrichment analysis (GSEA)  
121 (**Figure 2B**). The patients who developed VAP exhibited upregulation of pathways related to anti-  
122 bacterial immune responses, such as neutrophil degranulation, toll-like receptor signaling,  
123 cytokine signaling, and antigen presentation (**Figure 2B**). Interferon alpha/beta signaling was the  
124 most upregulated pathway, suggesting prolonged viral infection in patients with VAP. Ingenuity  
125 pathway analysis (IPA) additionally predicted broad activation of upstream inflammatory cytokines  
126 in patients who developed VAP, in particular IFN $\alpha$  and IFN $\gamma$  (**Figure 2C**).

127

### 128 **COVID-19 patients who develop VAP have attenuated immune signaling two weeks before** 129 **VAP onset**

130 Given our findings of a unique lower respiratory host transcriptional signature in the 48  
131 hours preceding VAP onset, we next asked whether differences in host immune signaling might  
132 exist even earlier, two or more weeks before clinical diagnosis of VAP, and whether such  
133 differences might explain the increased susceptibility to secondary bacterial infection in these

134 patients. We thus compared TA gene expression soon after the time of intubation between  
135 patients who eventually developed VAP (samples collected a median of two days post-intubation,  
136 17 days before VAP onset, n= 4) and patients who did not develop VAP (samples collected a  
137 median of two days after intubation, n = 8) (**Table 1**). We identified 154 differentially expressed  
138 genes at FDR <0.1. The COVID-19 patients who developed VAP had lower expression of several  
139 genes with roles in innate immunity including *IFI30*, *MMP2*, *TLR9*, and *DEFB124* (**Figure 3A**).  
140 GSEA further revealed that patients who developed VAP had lower expression of pathways  
141 related to antibacterial immune responses including neutrophil degranulation, toll-like receptor  
142 signaling, IL-17 signaling, antigen presentation and complement pathways and higher expression  
143 of IFN-alpha/beta signaling pathways, more than two weeks before the onset of VAP (**Figure 3B**).  
144 Additionally, pathways related to adaptive immunity such as T and B cell receptor signaling were  
145 also downregulated in patients who subsequently developed VAP (**Figure 3B**).

146 To gauge the degree of immune signaling suppression compared to controls, we  
147 performed a similar analysis on critically ill intubated patients without infection (**Figure 3C**).  
148 Relative to the control group, multiple antibacterial immune pathways were downregulated in  
149 COVID-19 patients, with the greatest attenuation in the VAP group (**Figure 3C**). Upstream  
150 regulator analysis identified impaired activation of diverse cytokines in those with VAP, while  
151 IFNB1 was notably upregulated (**Figure 3D**). Several pro-inflammatory cytokines were  
152 downregulated in both groups compared to the controls (**Figure S1**). We expanded the  
153 comparison at the “early” time-point to include patients with culture-negative VAP (VAP: n=6, No-  
154 VAP: n=11) and observed similar differences at the pathway level (**Figure S2**).

155 Given prior reports demonstrating correlation between SARS-CoV-2 viral load and  
156 interferon related gene expression<sup>14</sup> we next asked whether viral load differed between VAP and  
157 No-VAP patients. No differences in SARS-CoV-2 qPCR or viral reads per million (rpM) in bulk  
158 RNA-seq data were found in the days following intubation (P = 0.84 (RNA-seq), P = 0.53 (PCR),  
159 **Figure S3**). We also considered the possibility that differences in the number of days of steroid

160 exposure prior to sample collection might explain results, but found no differences ( $P = 0.343$ )  
161 **(Table S1)**.

162

163 **COVID-19 VAP is associated with impaired anti-bacterial immune signaling in monocytes,**  
164 **macrophages and neutrophils**

165 To further understand the mechanism of early downregulation of key pathways involved  
166 in antibacterial responses, we next asked whether this was driven by any one local immune cell  
167 type. We performed scRNA-seq on TA specimens obtained early during disease course (median  
168 of nine days before VAP) and enriched for immune cells using CD45 selection **(Methods)**.  
169 Clustering based upon cellular transcriptional signatures indicated that monocytes, macrophages  
170 and neutrophils were the most abundant cell types **(Figure 4A, S4A)** and thus we focused  
171 transcriptional assessment on these populations. A comparison of cell type proportions did not  
172 reveal statistically significant differences in populations of mono/macros, neutrophils or T cells in  
173 COVID-19 patients who subsequently developed VAP **(Figure 4B)**.

174 COVID-19 patients who developed VAP had distinct cell type-specific transcriptional  
175 signatures compared to those without VAP at this “early” post-intubation time-point **(Figure 4, S5,**  
176 **S6)**. With respect to mono/macros and neutrophils, we identified 532 and 693 differential expressed  
177 genes, respectively, at  $FDR < 0.05$ . Several genes with key roles in innate immunity were  
178 downregulated in both cell types in the COVID-19 patients who subsequently developed VAP  
179 versus those who did not, including *IL1Rn*, *ICAM1*, *NFKB2*, and *ITGAX* in neutrophils, as well as  
180 the neutrophil chemokines *CXCL2* and *CXCL8* in mono/macros **(Figure 4C, 4F, S5)**. In addition,  
181 similar to the bulk RNA-seq results demonstrating upregulation of type I IFN signaling at this time-  
182 point in patients who developed VAP, we noted upregulation of several interferon-induced genes  
183 including *IFI27* and *IFI30* in mono/macros, and *IFI30*, *IFITM1*, and *IFITM3* in neutrophils **(Figure**  
184 **4C, F)**.



185 IPA canonical pathway analysis of gene expression within each cluster revealed  
186 downregulation of several cytokine and innate immune signaling pathways in the patients who  
187 later developed VAP at the “early” post-intubation time-point. In the mono/mac cluster, this  
188 included downregulation of IL-1, IL-6, and iNOS signaling, as well as Th17 and TNFR2 signaling  
189 **(Figure 4D)**. Analysis of the neutrophil cluster also demonstrated attenuated IL-1, IL-6, and  
190 TNFR2 signaling and NF-κB pathways **(Figure 4G)**. COVID-19 patients who subsequently  
191 developed VAP demonstrated upregulation of oxidative phosphorylation and glutathione  
192 detoxification in the mono/mac subset, and interferon signaling, oxidative phosphorylation and  
193 EIF2 signaling in the neutrophil cluster. Computational prediction of upstream cytokine activation  
194 by IPA revealed impaired activation of multiple pro-inflammatory cytokines in both the mono/macs  
195 and neutrophils in patients who developed VAP, including TNF, CXCL8, and IL1B, as well as  
196 downregulation of key factors important in monocyte to macrophage differentiation (*CSF2*, *CSF3*,  
197 *PF4*) **(Figure 4E, H)**.

198 In the T cell population, we identified 1318 differentially expressed genes at FDR < 0.05.  
199 Genes associated with T cell recruitment, including *CXCR6*, *ITGA1* and *ITGA4*, which have been  
200 shown to regulate localization and retention of T cells in the lung during viral infection<sup>15,16</sup>, were  
201 downregulated in patients with VAP. Additionally, genes indicative of T cell activation (*CD69*,  
202 *CD96*, *LAG3*, *ICOS*, *CD27*), signaling (*CD3*, *ZAP70*, *ITK*, *CD8A*, *CD8B*), and effector functions  
203 (*IFNG*, *GZMA*, *GZMB*, *KLRG1*) were significantly downregulated in patients with VAP, suggesting  
204 an impairment in T cell responses **(Figure S6A)**. IPA revealed downregulation of signaling  
205 pathways crucial for T cell recruitment, such as integrin signaling, and activation, such as CD28  
206 signaling in helper T cells and phospholipase C signaling **(Figure S6B)**.

207

## 208 **Temporal dynamics of the host response in COVID-19 patients who develop VAP**

209 We next investigated temporal dynamics of the lower airway host inflammatory response  
210 in COVID-19 patients from the time of intubation to development of VAP by evaluating differential

211 gene expression between COVID-19 VAP patients at the “early” time point (median of 17 days  
212 before VAP onset, n=4) versus “late” time point (median of two days before VAP onset, n=5) by  
213 bulk RNA-seq. We identified 2705 differentially expressed genes (FDR<0.1) and unsupervised  
214 hierarchical clustering of the 50 most significant genes demonstrated clear separation of the two  
215 time-points (**Figure 5A**). GSEA revealed that type I interferon signaling was notably  
216 downregulated at the “late” time-point most immediately preceding VAP onset in comparison to  
217 the “early” timepoint (**Figure 5B**); however, expression was still significantly higher than in the  
218 No-VAP patients (**Figure 2B**). Several other immune signaling pathways were more highly  
219 expressed at this “late” time-point, presumably reflecting activation of an antibacterial response  
220 in the setting of bacterial pneumonia (**Figure 5B**). Consistent with this, upstream regulator  
221 analysis indicated increased activation of several pro-inflammatory cytokines and decreased  
222 IFN $\alpha$  and IFN- $\lambda$  signaling at the “late” versus “early” time-points (**Figure 5C**).

223 In contrast, comparing No-VAP patients at the “early” (n=8) versus “late” (n=8) time-points  
224 yielded only two genes with a padj <0.1, both of which were interferon-stimulated genes (*RSAD2*  
225 and *CMPK2*) downregulated at the “late” time-point, suggesting that while the host response was  
226 relatively unchanged in these patients, the antiviral response attenuated over time. Indeed, GSEA  
227 revealed that type I interferon signaling, and other antiviral immune pathways were downregulated  
228 in the patients who did not develop VAP at the later time-point (**Figure S7**).

229 Next, we performed a similar comparison between the “early” and “late” time-points based  
230 on scRNA-seq data from patients who developed VAP. Differential gene expression analysis on  
231 these two populations identified 1368 differentially expressed genes (FDR<0.05) in the mono/mac  
232 cluster, and 1028 in the neutrophil cluster. IPA revealed upregulation of antibacterial signaling  
233 pathways at the later time-point, including signaling by several cytokines in the mono/mac cluster  
234 (IL-17, IL-6, IL-1, TNF, IL-23, IFN) (**Figure 5D-E**), congruent with the bulk RNA-seq analysis.  
235 Furthermore, we identified 1397 differentially expressed genes (FDR < 0.05) in the T cell cluster  
236 between the two time-points and noted upregulation of signaling pathways indicative of an active

237 T cell response<sup>17</sup> (e.g. ERK/MAPK, Tec kinase, and phospholipase C) in the days preceding VAP,  
238 which was also in agreement with the bulk RNA-seq results (**Figure S6C**).

239 We further assessed dynamics of host immune responses between VAP and No-VAP  
240 patients by performing longitudinal analyses of key immune signaling pathways, including all  
241 patients with available TA samples (VAP n=7, No-VAP n=10). Onset of VAP in these patients  
242 ranged from 10-39 days post intubation, with a median of 25 days, and treatment with  
243 immunosuppressants did not differ significantly between VAP and no-VAP patients ( $p=0.304$ ,  
244 Fisher's exact test). We calculated pathway Z-scores for each sample by averaging Z-scores for  
245 the top 20 leading edge genes of each pathway (**Methods**). Early attenuation of immune signaling  
246 in the VAP group was conspicuous, and this pattern eventually resolved later in disease course  
247 by the time secondary bacterial infection became established (**Figures 5E-H**). We confirmed that  
248 the observed differences between VAP and no-VAP patients were not driven by differences in  
249 treatment with immunosuppressants by comparing pathway Z-scores in patients that received  
250 immunosuppressants and those that did not at the early time-point regardless of VAP group  
251 (**Figure S8**).

252

### 253 **Lung microbiome disruption precedes VAP in COVID-19 patients**

254 We hypothesized that the innate immune suppression in patients who developed VAP  
255 would correlate with viral load. Using TA metatranscriptomics to assess the lower respiratory  
256 microbiome, we evaluated longitudinal changes in SARS-CoV-2 abundance. Although no  
257 difference was observed at the "early" timepoint (**Figure S3**), the trajectory of SARS-CoV-2 viral  
258 load differed significantly in patients who developed VAP ( $p=0.0058$ ), although in both groups  
259 decreased over time (**Figure 6A**). This result suggested that COVID-19 patients who develop  
260 VAP may exhibit impaired ability to clear virus compared to those who do not, and that the lung  
261 microbiome composition may be similarly impacted.

262           Indeed, COVID-19 patients who developed VAP exhibited a significant reduction in  
263 bacterial diversity of their airway microbiome up to three weeks before clinical signs of infection  
264 (Shannon Diversity Index,  $p=0.012$ ; **Figure 6B**). COVID-19 patients who developed VAP also had  
265 lower airway microbiome compositions more closely resembling each other than those from  
266 patients who did not develop VAP, across all timepoints since intubation (Bray Curtis index,  
267  $p=0.0033$ ; **Figure 6C**), suggesting community collapse precedes the development of VAP. All  
268 patients received antibiotics prior to collection of the first sample, suggesting that antibiotic use  
269 was not driving these differences (**Table S1**).

270

## 271 **Discussion**

272           Secondary bacterial pneumonia contributes to significant morbidity and mortality in  
273 patients with primary viral lower respiratory tract infections<sup>1,3</sup>, but mechanisms governing  
274 individual susceptibility to VAP have remained unclear. Few human cohort studies have evaluated  
275 the immunologic underpinnings of VAP, and none have been reported in the context of COVID-  
276 19, which is characterized by a dysregulated host response distinct from other viral  
277 pneumonias<sup>14,18,19</sup>. To address this gap and probe mechanisms of VAP susceptibility in patients  
278 with COVID-19, we carried out a systems biological assessment of host and microbial dynamics  
279 of the lower respiratory tract.

280           Two days before VAP onset, a transcriptional signature consistent with bacterial infection  
281 was observed. This finding suggests that host response changes can occur before clinical  
282 recognition of pneumonia, highlighting the potential utility of the host transcriptome as a tool for  
283 VAP surveillance. While intriguing, this observation did not provide an explanation for differential  
284 susceptibility of some COVID-19 patients to post-viral pneumonia.

285           The discovery of an early suppressed antibacterial immune response in patients who later  
286 developed VAP did however, offer a potential explanation. More than two weeks before VAP  
287 onset, we observed a striking suppression of pathways related to both innate and adaptive

288 immunity, including neutrophil degranulation, TLR signaling, complement activation, antigen  
289 presentation, and T cell receptor and B receptor signaling, as well as cytokine signaling (e.g. IL-  
290 1, IL-4, IL-12, IL-13 and IL-17). Comparison against uninfected, intubated controls confirmed the  
291 previously described paradoxical impairment in immune signaling found in patients with severe  
292 COVID-19<sup>18</sup>, and suggested that VAP susceptibility may be the result of disproportionate  
293 suppression of innate and adaptive pathways critical for antibacterial defense, resulting in  
294 enhanced susceptibility to opportunistic secondary infections.

295         Animal models of influenza have provided insight into potential mechanisms of post-viral  
296 pneumonia, although none have provided insight regarding why some individuals are more  
297 susceptible than others. In mice inoculated with influenza, for instance, virus-induced type I IFN  
298 suppresses neutrophil chemokines and impairs Th17 immunity, compromising effective clearance  
299 of bacterial infections<sup>9,10</sup>. Interestingly, we also observed increased type I interferon signaling in  
300 COVID-19 patients who weeks later developed VAP, and a strikingly similar impairment in Th17  
301 signaling and other immune pathways. Desensitization to toll-like receptor (TLR) ligands after  
302 influenza infection has also been documented<sup>20</sup>, which is congruent with the downregulation of  
303 TLR signaling at the time of intubation observed in our bulk RNA-seq analyses.

304         Impaired bacterial clearance by alveolar macrophages was found to be driven by virus-  
305 related IFN $\gamma$  production by T cells<sup>21</sup> in a murine post-influenza model. In contrast, we found that  
306 T cells from patients who later developed VAP expressed lower levels of IFN $\gamma$  at the time of  
307 intubation. This difference may relate to species-specific variations in immune signaling or intrinsic  
308 differences in the host response to influenza virus versus SARS-CoV-2<sup>14,18</sup>.

309         We asked whether certain cell types were responsible for driving the early suppression of  
310 immune signaling observed in COVID-19 patients who went on to develop VAP. No significant  
311 differences in proportions of the most abundant cell types - monocytes/macrophages, neutrophils  
312 or T cells – was observed between patients with or without VAP at the time of intubation. This

313 finding suggests that an impairment of immune cell recruitment was not causing these differences,  
314 but rather significant gene expression differences within each of these immune cell populations.

315 In both the mono/mac and neutrophil populations, we observed broad downregulation of  
316 the innate immune response, and initiation of the adaptive immune response, concordant with  
317 global observations in bulk RNA-seq analyses. Further analysis revealed a downregulation of  
318 monocyte to macrophage differentiation and neutrophil chemotaxis. Further, we noted a  
319 downregulation of key pathways and transcription factors involved in antimicrobial immune  
320 responses including iNOS in mono/macs, as well as NFkB and TREM1 in mono/macs and  
321 neutrophils. Both bulk and scRNA-seq suggested an impairment in T cell recruitment, signaling,  
322 and effector functions. Overall, our data suggest that while no difference in cell type populations  
323 existed between groups, changes in the gene expression of mono/macs, neutrophils and T cells  
324 contributes to immune suppression in COVID-19 patients who later develop VAP.

325 SARS-CoV-2 viral load correlates with interferon stimulated gene expression<sup>14,18</sup> and thus  
326 we initially hypothesized that differences in viral load between groups might relate to individual  
327 VAP susceptibility. However, we found no difference between groups at the “early” timepoint.  
328 Moreover, no differences existed in terms of immunosuppressive medication administration or  
329 clinically diagnosed immunodeficiency, suggesting that other, still unidentified mechanisms  
330 present at the time of intubation must underlie the marked suppression of immune gene  
331 expression in COVID-19 patients who went on to develop VAP.

332 While no difference in viral load was observed at the time of intubation, the COVID-19  
333 patients who developed VAP exhibited impaired viral clearance over the time-course of intubation.  
334 This observation was corroborated by a prolonged antiviral type I interferon response at the “late”  
335 timepoint (median of two days before VAP onset) in patients who developed VAP versus those  
336 who did not, pointing to the persistence of suboptimal antiviral immunity in these patients. Early  
337 induction of functional SARS-CoV-2 specific T cells is associated with faster viral clearance in

338 COVID-19 patients<sup>22</sup> and likewise, we observed impairments in T cell activation and signaling in  
339 the VAP group, which further suggests a decreased ability to control the virus in these patients.

340         Respiratory viruses can reshape the human airway microbiome by modulating host  
341 inflammatory responses<sup>23,24</sup>. In mouse models of influenza, the airway microbiome exhibits  
342 expansion of several bacterial families during the course of viral infection as innate immunity is  
343 suppressed<sup>23</sup>. These changes increase the risk of secondary bacterial infection<sup>23</sup> and have been  
344 observed in patients with chronic obstructive pulmonary disease, where suppression of the innate  
345 immune response in rhinovirus infected patients may be followed by bacterial superinfection<sup>25,26</sup>.

346         Similarly, the innate immune suppression observed in COVID-19 patients who developed  
347 VAP was associated with airway microbiome collapse and the outgrowth of lung pathogens in  
348 advance of clinical VAP diagnosis. This finding suggests that individual immune responses to  
349 SARS-CoV-2 infection may drive a restructuring of the microbial community and increase  
350 susceptibility to VAP (**Figure 7**). The resulting outgrowth of a VAP-associated bacterial pathogen  
351 may elicit an antibacterial response, but the broader immunosuppressive state preceding this  
352 response may be insufficient to control the development of clinical pneumonia. Those with a  
353 lesser degree of immunosuppression may be able to respond faster and therefore control  
354 opportunistic bacterial pathogens more effectively.

355         These findings may also have important implications for management of patients with  
356 COVID-19 related acute respiratory failure, many of whom are now being treated with  
357 corticosteroids plus/minus IL-6 receptor blocking agents. These agents may lead to further  
358 suppression of the key pathways required for host response to secondary bacterial infection.  
359 Thus, our results emphasize the need for ongoing vigilance for VAP in patients treated with potent  
360 immunosuppressive agents, as well as the need to develop novel diagnostic and/or prognostic  
361 approaches to identifying patients at highest risk. For instance, availability of molecular  
362 biomarkers to assess a patient's risk of VAP at the time of intubation could reduce inappropriate  
363 use of prophylactic antibiotics or immunomodulatory treatments, or signal a need for enhanced

364 surveillance strategies. Signatures of immune dysfunction have been used as biomarkers to  
365 predict nosocomial infection in critically ill patients,<sup>27</sup> although not in the context of viral infection.

366 Sample size is a limitation of this study; however, the reproducibility of our observations  
367 across both bulk and scRNA-seq analyses and the significant number of differentially expressed  
368 genes among the comparator groups support the validity of our conclusions. Because this study  
369 was limited to critically ill, intubated patients, we were unable to assess early stages of COVID-  
370 19, which may provide additional insight regarding determinants of secondary bacterial infection.  
371 Additionally, we were unable to assess whether epithelial cells contributed to VAP risk due to  
372 enrichment for immune cells prior to scRNA-seq. With larger cohorts, the early detection of  
373 specific immune pathway suppression and microbiome collapse could be leveraged to develop  
374 clinically useful models for identifying COVID-19 patients with increased susceptibility to  
375 secondary bacterial pneumonia.

376

## 377 **Materials and Methods**

378

### 379 **Study design, cohorts, enrollment and ethics approval**

380 We conducted a prospective case-control study of adults requiring mechanical ventilation  
381 for COVID-19 with or without secondary bacterial pneumonia. We also evaluated control patients  
382 requiring mechanical ventilation for other reasons who had no evidence of pulmonary infection  
383 (**Figure 1**). Patients were enrolled in either of two prospective cohort studies of critically ill patients  
384 at the University of California, San Francisco (UCSF) and Zuckerberg San Francisco General  
385 Hospital between 07/2013 and 07/2020. Both cohort studies were approved by the UCSF  
386 Institutional Review Board (IRB) under protocols 10-02701 (control patients, pre-COVID-19  
387 pandemic) and 20-30497 (COVID-19 patients, COVID-19 Multiphenotyping for Effective Therapy  
388 (COMET) study), respectively. Of the COVID-19 patients, 19 were co-enrolled in the National



389 Institute of Allergy and Infectious Diseases-funded Immunophenotyping Assessment in a COVID-  
390 19 Cohort (IMPACC) Network study.

391 For both the COVID-19 and control cohorts, if a patient met inclusion criteria, then a study  
392 coordinator or physician obtained written informed consent for enrollment from the patient or their  
393 surrogate. Patients or their surrogates were provided with detailed written and verbal information  
394 about the goals of the study, the data and specimens that would be collected, and the potential  
395 risks to the subject. Patients and their surrogates were also informed that there would be no  
396 benefit to them from being enrolled in the study and that they may withdraw informed consent at  
397 any time during the course of the study. All questions were answered, and informed consent  
398 documented by obtaining the signature of the patient or their surrogate on the consent document  
399 (or during the COVID-19 pandemic, the IRB-approved electronic equivalent, to enable touchless  
400 consent).

401 Many critically ill patients are unconscious at the time of intensive care unit (ICU)  
402 admission due to their underlying illness and/or are endotracheally intubated for airway  
403 management or acute respiratory failure. The patients who are not unconscious are often in pain  
404 and may have acute delirium due to critical illness and/or medications. For these reasons, many  
405 subjects are unable to provide informed consent at the time of enrollment. Because this study  
406 could not practically be done otherwise and was deemed to be minimal risk by the UCSF IRB, if  
407 a patient was unable and a surrogate was not available to provide consent, patients were enrolled  
408 with waiver of initial consent, including the collection of biological samples.

409 Specifically, for subjects who were unable to provide informed consent at the time of  
410 enrollment, our study team was permitted to collect biological samples as well as clinical data  
411 from the medical record obtained prior to consent. Surrogate consent was vigorously pursued for  
412 all patients; moreover, each patient was regularly examined to determine if and when s/he was  
413 able to consent for him/herself, and the nursing and ICU staff were contacted daily for information

414 about surrogates' availability. For patients whose surrogates provided informed consent, follow-  
415 up consent was subsequently obtained from the patient if they survived their acute illness and  
416 regained the ability to consent. For subjects who died prior to the consent being obtained, a full  
417 waiver of consent was approved by the UCSF IRB for both cohort studies. Lack of a surrogate to  
418 provide consent is common in critically ill patients. To address this, the UCSF IRB also approved  
419 a full waiver of consent for subjects in the COVID-19 cohort who remained unable to provide  
420 informed consent and had no contactable surrogate identified within 28 days. Before utilizing this  
421 waiver, we made and documented at least three separate attempts to identify and contact the  
422 patient or surrogate over a month-long period. While most patients enrolled were consented by  
423 typical processes, three died prior to consent being obtained, and five were included with a full  
424 waiver of consent due to lack of ability to consent and lack of contactable surrogate. No personally  
425 identifiable information has been included as part of this manuscript for any enrolled patients.

426

#### 427 **Ventilator-associated pneumonia adjudication**

428 A total of 84 adults who required intubation for severe COVID-19 (Cohort 1) and who had  
429 available TA samples were considered for inclusion in the study (**Figure 1**). Patients who met the  
430 Centers for Disease Control (CDC) definition for VAP<sup>13</sup> with a positive bacterial sputum culture  
431 were adjudicated as having VAP for the purpose of the study (N=16); patients who did not meet  
432 these criteria, and for whom there was no sustained clinical suspicion for bacterial pneumonia  
433 during the admission, were categorized as No-VAP (N=17). VAP and No-VAP patients for whom  
434 samples at the time-points of interest were available were included in the primary analyses (VAP:  
435 N=10; No-VAP: N=13). Patients who met CDC-VAP criteria but had negative TA cultures were  
436 included in a secondary supplementary analysis only (N=5). All other patients were excluded,  
437 including patients with clinically-suspected bacterial pneumonia who did not meet CDC VAP  
438 criteria. Eight intubated patients from a recent study<sup>18</sup> (Cohort 2) were included as controls and

439 were selected because they had previously been adjudicated as having no evidence of lower  
440 respiratory tract infection. This group included four patients with the acute respiratory distress  
441 syndrome (ARDS) due to non-infectious etiologies, and four patients without ARDS who were  
442 intubated for other reasons (subdural hematoma (N=1), retroperitoneal hemorrhage (N=1), or  
443 neurosurgical procedures (N=2)).

444

#### 445 **Tracheal aspirate sampling**

446 Following enrollment, tracheal aspirate (TA) was collected (periodically following  
447 intubation for Study 1, or once within 3 days of intubation for Study 2), without addition of saline  
448 wash, and either a) mixed 1:1 with DNA/RNA shield (Zymo Research) for bulk RNA-seq or b)  
449 immediately processed in a biosafety level 3 laboratory (BSL3) for scRNA-seq analysis.

450

#### 451 **Bulk RNA sequencing and host transcriptome analysis**

452

##### 453 RNA sequencing

454 To evaluate host and microbial gene expression, metatranscriptomic next generation RNA  
455 sequencing (RNA-seq) was performed on TA specimens. Following RNA extraction (Zymo  
456 Pathogen Magbead Kit) and DNase treatment, human cytosolic and mitochondrial ribosomal RNA  
457 was depleted using FastSelect (Qiagen). To control for background contamination, we included  
458 negative controls (water and HeLa cell RNA) as well as positive controls (spike-in RNA standards  
459 from the External RNA Controls Consortium (ERCC))<sup>28</sup>. RNA was then fragmented and  
460 underwent library preparation using the NEBNext Ultra II RNA-seq Kit (New England BioLabs).  
461 Libraries underwent 146 nucleotide paired-end Illumina sequencing on an Illumina Novaseq 6000.

462

463 Host differential expression

464           Following demultiplexing, sequencing reads were pseudo-aligned with kallisto<sup>29</sup> to an  
465 index consisting of all transcripts associated with human protein coding genes (ENSEMBL v.  
466 99), cytosolic and mitochondrial ribosomal RNA sequences and the sequences of ERCC RNA  
467 standards. Gene-level counts were generated from the transcript-level abundance estimates  
468 using the R package tximport<sup>30</sup>, with the scaledTPM method. Samples retained in the dataset  
469 had a total of at least 1,000,000 estimated counts associated with transcripts of protein coding  
470 genes.

471           Genes were retained for differential expression analysis if they had counts in at least 30%  
472 of samples. Differential expression analysis was performed using the R package DESeq2<sup>31</sup>. We  
473 modeled the expression of individual genes using the design formula ~VAPgroup, where VAP  
474 groups were “VAP-early”, “No VAP-early”, “VAP-late” and “No VAP-late” and used the results()  
475 function to extract a specific contrast. Separate comparisons to the control group were performed  
476 using the design formula ~COVID-19-status to compare positive and negative patients.

477           Significant genes were identified using a Benjamini-Hochberg false discovery rate (FDR)  
478 < 0.1. We generated heatmaps of the top 50 differentially expressed genes by FDR. For  
479 visualization, gene expression was normalized using the regularized log transformation, centered,  
480 and scaled prior to clustering. Heatmaps were generated using the *pheatmap* package. Columns  
481 were clustered using Euclidean distance and rows were clustered using Pearson correlation.  
482 Differential expression analysis results are provided in (**Supplementary data file 1**).

483

484 Pathway analysis

485           Gene set enrichment analyses (GSEA) were performed using the fgseaMultilevel function  
486 in the R package fgsea<sup>32</sup> and REACTOME pathways<sup>33</sup> with a minimum size of 10 genes and a  
487 maximum size of 1,500 genes. All genes were included in the comparison, pre-ranked by the test  
488 statistic. Significant pathways were defined as those with a Benjamini-Hochberg adjusted p-value

489 < 0.05. Ingenuity Pathway Analysis (IPA) Canonical Pathway and Upstream Regulator Analysis<sup>34</sup>  
490 was employed on genes with  $p < 0.1$  and ranked by the test statistic to identify cytokine regulators.  
491 Significant IPA results were defined as those with a Z-score absolute value greater than 2 and an  
492 overlap P value < 0.05. The gene sets in figures were selected to reduce redundancy and highlight  
493 diverse biological functions. Full GSEA and IPA results are provided in (**Supplementary data**  
494 **files 2 and 3**).

495 Longitudinal pathway analysis was performed using all available TA samples spanning  
496 post-intubation to VAP onset for all patients included in the bulk RNA-seq analysis. Analysis was  
497 restricted to samples with at least 1,000,000 human protein coding transcripts. Pathways of  
498 interest were selected from the significant GSEA results of the comparison of VAP vs. No-VAP  
499 patients in the “early” time-point. The top 20 leading edge genes were selected from each pathway  
500 for analysis. To calculate a Z-score for each gene, expression was normalized using the variance  
501 stabilizing transformation (VST), centered, and scaled. A pathway Z-score was calculated by  
502 averaging the 20 gene Z-scores. Multiple Z-scores per patient at a given time interval were  
503 averaged so that each patient corresponds to one datapoint at each interval. Statistical  
504 significance of pathway expression over time between VAP and No-VAP groups was calculated  
505 using a two-way analysis of variance (ANOVA) in GraphPad PRISM.

506

### 507 **Single cell RNA sequencing and transcriptome analysis**

508 After collection, fresh TA was transported to a BSL-3 laboratory at ambient temperature  
509 to improve neutrophil survival. 3mL of TA was dissociated in 40mL of PBS with 50ug/mL  
510 collagenase type 4 (Worthington) and 0.56 ku/mL of Dnase I (Worthington) for 10 minutes at room  
511 temperature, followed by passage through a 70 $\mu$ M filter. Cells were pelleted at 350g 4C for 10  
512 minutes, resuspended in PBS with 2mM EDTA and 0.5% BSA, and manually counted on a  
513 hemocytometer. Cells were stained with MojoSort Human CD45 and purified by the  
514 manufacturer’s protocol (Biolegend). After CD45 positive selection, cells were manually counted

515 with trypan blue on a hemocytometer. Using a V(D)J v1.1 kit according to the manufacturer's  
516 protocol, samples were loaded on a 10X Genomics Chip A without multiplexing, aiming to capture  
517 10,000 cells (10X Genomics). Libraries underwent paired end 150 base pair sequencing on an  
518 Illumina NovaSeq6000.

519 Raw sequencing reads were aligned to GRCh38 using the STAR aligner<sup>35</sup>. Cell barcodes  
520 were then determined based upon UMI count distribution. Read count matrices were generated  
521 through the 10X genomics cellranger pipeline v3.0. Data was processed and analyzed using the  
522 Scanpy v1.6<sup>36</sup>. Cells that had <200 genes and had greater than 30,000 counts were filtered.  
523 Mitochondrial genes were removed and multi-sample integration was performed using Harmony  
524 v0.1.4<sup>37</sup>. Differential expression was performed using MAST v1.16.0<sup>38</sup>. Due to the significantly  
525 greater number of differentially expressed genes in scRNA-seq analyses, we used a more  
526 restrictive cutoff of FDR < 0.05 for significant genes. Differential expression analysis results are  
527 detailed in (**Supplementary data file 4**).

528

#### 529 Pathway analysis

530 Ingenuity Pathway Analysis (IPA) Canonical Pathway and Upstream Regulator Analysis<sup>34</sup>  
531 was employed on genes with  $p < 0.05$  and ranked by  $\log_2$ foldchange to identify canonical pathways  
532 and cytokine regulators. We utilized a more restrictive  $p$  value cutoff for scRNA-seq to ensure a  
533 similar number of genes were input into IPA. Significant IPA results were defined as those with a  
534 Z-score absolute value greater than 2 and an overlap  $P$  value < 0.05. The gene sets in figures  
535 were selected to reduce redundancy and highlight diverse biological functions. Full GSEA and  
536 IPA results are provided in (**Supplementary data files 5 and 6**).

537

#### 538 **Lung microbiome analysis**

539 RNA from tracheal aspirates was sequenced as described above. Taxonomic alignments  
540 were obtained from raw sequencing reads using the IDseq pipeline<sup>39,40</sup>, which performs quality

541 filtration and removal of human reads followed by reference-based taxonomic alignment at both  
542 the nucleotide and amino acid level against sequences in the National Center for Biotechnology  
543 Information (NCBI) nucleotide (NT) and non-redundant (NR) databases, followed by assembly of  
544 reads matching each taxon detected. Taxonomic alignments underwent background correction  
545 for environmental contaminants (see below), viruses were excluded, and data was then  
546 aggregated to the genus level before calculating diversity metrics. Alpha diversity (Shannon's  
547 Diversity Index) and beta diversity (Bray-Curtis dissimilarity) were calculated and the latter plotted  
548 using non-metric multidimensional scaling (NDMS). Comparison of alpha and beta diversity over  
549 time between VAP and No-VAP groups was calculated using a two-way analysis of variance  
550 (ANOVA) in GraphPad PRISM.

551

#### 552 Identification and mitigation of environmental contaminants

553 To minimize inaccurate taxonomic assignments due to environmental and reagent derived  
554 contaminants, non-templated "water only" and HeLa cell RNA controls were processed with each  
555 group of samples that underwent nucleic acid extraction. These were included, as well as positive  
556 control clinical samples, with each sequencing run. Negative control samples enabled estimation  
557 of the number of background reads expected for each taxon. A previously developed negative  
558 binomial model<sup>14</sup> was employed to identify taxa with NT sequencing alignments present at an  
559 abundance significantly greater compared to negative water controls. This was done by modeling  
560 the number of background reads as a negative binomial distribution, with mean and dispersion  
561 fitted on the negative controls. For each batch (sequencing run) and taxon, we estimated the  
562 mean parameter of the negative binomial by averaging the read counts across all negative  
563 controls, slightly regularizing this estimate by including the global average (across all batches) as  
564 an additional sample. We estimated a single dispersion parameter across all taxa and batches,  
565 using the functions `glm.nb()` and `theta.md()` from the R package MASS<sup>41</sup>. Taxa that achieved a p-  
566 value <0.01 were carried forward.

567 **References**

- 568 1. Falsey, A. R. *et al.* Bacterial Complications of Respiratory Tract Viral Illness: A  
569 Comprehensive Evaluation. *The Journal of Infectious Diseases* **208**, 432–441 (2013).
- 570 2. Morens, D. M., Taubenberger, J. K. & Fauci, A. S. Predominant role of bacterial pneumonia  
571 as a cause of death in pandemic influenza: implications for pandemic influenza  
572 preparedness. *J Infect Dis* **198**, 962–970 (2008).
- 573 3. Rouzé, A. *et al.* Relationship between SARS-CoV-2 infection and the incidence of ventilator-  
574 associated lower respiratory tract infections: a European multicenter cohort study. *Intensive*  
575 *Care Med* 1–11 (2021) doi:10.1007/s00134-020-06323-9.
- 576 4. Luyt, C.-E. *et al.* Ventilator-associated pneumonia in patients with SARS-CoV-2-associated  
577 acute respiratory distress syndrome requiring ECMO: a retrospective cohort study. *Ann*  
578 *Intensive Care* **10**, 158 (2020).
- 579 5. Bardi, T. *et al.* Nosocomial infections associated to COVID-19 in the intensive care unit:  
580 clinical characteristics and outcome. *Eur J Clin Microbiol Infect Dis* (2021)  
581 doi:10.1007/s10096-020-04142-w.
- 582 6. Maes, M. *et al.* Ventilator-associated pneumonia in critically ill patients with COVID-19. *Crit*  
583 *Care* **25**, 25 (2021).
- 584 7. Søgaaard, K. K. *et al.* Community-acquired and hospital-acquired respiratory tract infection  
585 and bloodstream infection in patients hospitalized with COVID-19 pneumonia. *J Intensive*  
586 *Care* **9**, (2021).
- 587 8. Metzger, D. W. & Sun, K. Immune Dysfunction and Bacterial Co-Infections following  
588 Influenza. *J Immunol* **191**, 2047–2052 (2013).
- 589 9. Shahangian, A. *et al.* Type I IFNs mediate development of postinfluenza bacterial pneumonia  
590 in mice. *J Clin Invest* **119**, 1910–1920 (2009).
- 591 10. Kudva, A. *et al.* Influenza A inhibits Th17-mediated host defense against bacterial  
592 pneumonia in mice. *J Immunol* **186**, 1666–1674 (2011).



- 593 11. Langelier, C. *et al.* Integrating host response and unbiased microbe detection for lower  
594 respiratory tract infection diagnosis in critically ill adults. *Proc Natl Acad Sci U S A* **115**,  
595 E12353–E12362 (2018).
- 596 12. Flanagan, J. L. *et al.* Loss of bacterial diversity during antibiotic treatment of intubated  
597 patients colonized with *Pseudomonas aeruginosa*. *J Clin Microbiol* **45**, 1954–1962 (2007).
- 598 13. CDC-NHSN. Pneumonia (Ventilator-associated [VAP] and non-ventilator-associated  
599 Pneumonia [PNEU]) Event.
- 600 14. Mick, E. *et al.* Upper airway gene expression reveals suppressed immune responses to  
601 SARS-CoV-2 compared with other respiratory viruses. *Nature Communications* **11**, 5854  
602 (2020).
- 603 15. Wein, A. N. *et al.* CXCR6 regulates localization of tissue-resident memory CD8 T cells to the  
604 airways. *Journal of Experimental Medicine* **216**, 2748–2762 (2019).
- 605 16. Grau, M. *et al.* Antigen-Induced but Not Innate Memory CD8 T Cells Express NKG2D and  
606 Are Recruited to the Lung Parenchyma upon Viral Infection. *The Journal of Immunology*  
607 **200**, 3635–3646 (2018).
- 608 17. Smith-Garvin, J. E., Koretzky, G. A. & Jordan, M. S. T cell activation. *Annu Rev Immunol* **27**,  
609 591–619 (2009).
- 610 18. Sarma, A. *et al.* COVID-19 ARDS is characterized by a dysregulated host response that  
611 differs from cytokine storm and is modified by dexamethasone. *Res Sq* (2021)  
612 doi:10.21203/rs.3.rs-141578/v1.
- 613 19. Blanco-Melo, Daniel. Imbalanced host response to SARS-CoV-2 drives development of  
614 COVID-19. *Cell*. doi:10.1016/j.cell.2020.04.026.
- 615 20. Didierlaurent, A. *et al.* Sustained desensitization to bacterial Toll-like receptor ligands after  
616 resolution of respiratory influenza infection. *J Exp Med* **205**, 323–329 (2008).
- 617 21. Sun, K. & Metzger, D. W. Inhibition of pulmonary antibacterial defense by interferon-gamma  
618 during recovery from influenza infection. *Nat Med* **14**, 558–564 (2008).

- 619 22. Tan, A. T. *et al.* Early induction of functional SARS-CoV-2-specific T cells associates with  
620 rapid viral clearance and mild disease in COVID-19 patients. *Cell Reports* **34**, 108728  
621 (2021).
- 622 23. Goulding, J. *et al.* Lowering the Threshold of Lung Innate Immune Cell Activation Alters  
623 Susceptibility to Secondary Bacterial Superinfection. *J Infect Dis* **204**, 1086–1094 (2011).
- 624 24. Man, W. H., de Steenhuijsen Piters, W. A. A. & Bogaert, D. The microbiota of the respiratory  
625 tract: gatekeeper to respiratory health. *Nat Rev Microbiol* **15**, 259–270 (2017).
- 626 25. Mallia, P. *et al.* Rhinovirus Infection Induces Degradation of Antimicrobial Peptides and  
627 Secondary Bacterial Infection in Chronic Obstructive Pulmonary Disease. *Am J Respir Crit*  
628 *Care Med* **186**, 1117–1124 (2012).
- 629 26. Molyneaux, P. L. *et al.* Outgrowth of the Bacterial Airway Microbiome after Rhinovirus  
630 Exacerbation of Chronic Obstructive Pulmonary Disease. *Am J Respir Crit Care Med* **188**,  
631 1224–1231 (2013).
- 632 27. Conway Morris, A. *et al.* Cell-surface signatures of immune dysfunction risk-stratify critically  
633 ill patients: INFECT study. *Intensive Care Med* **44**, 627–635 (2018).
- 634 28. Pine, P. S. *et al.* Evaluation of the External RNA Controls Consortium (ERCC) reference  
635 material using a modified Latin square design. *BMC Biotechnol* **16**, 54 (2016).
- 636 29. Bray, N. L., Pimentel, H., Melsted, P. & Pachter, L. Near-optimal probabilistic RNA-seq  
637 quantification. *Nature Biotechnology* **34**, 525–527 (2016).
- 638 30. Sonesson, C., Love, M. I. & Robinson, M. D. Differential analyses for RNA-seq: transcript-  
639 level estimates improve gene-level inferences. *F1000Res* **4**, 1521 (2015).
- 640 31. Love, M. I., Huber, W. & Anders, S. Moderated estimation of fold change and dispersion for  
641 RNA-seq data with DESeq2. *Genome Biol* **15**, 550 (2014).
- 642 32. Korotkevich, G., Sukhov, V. & Sergushichev, A. Fast gene set enrichment analysis. *bioRxiv*  
643 060012 (2019) doi:10.1101/060012.

- 644 33. Croft, D. *et al.* The Reactome pathway knowledgebase. *Nucleic Acids Res* **42**, D472-477  
645 (2014).
- 646 34. Krämer, A., Green, J., Pollard, J. & Tugendreich, S. Causal analysis approaches in  
647 Ingenuity Pathway Analysis. *Bioinformatics* **30**, 523–530 (2014).
- 648 35. Dobin, A. *et al.* STAR: ultrafast universal RNA-seq aligner. *Bioinformatics* **29**, 15–21 (2013).
- 649 36. Wolf, F. A., Angerer, P. & Theis, F. J. SCANPY : large-scale single-cell gene expression  
650 data analysis. *Genome Biology* **19**, 15 (2018).
- 651 37. Korsunsky, I. *et al.* Fast, sensitive, and accurate integration of single cell data with  
652 Harmony. *bioRxiv* 461954 (2018) doi:10.1101/461954.
- 653 38. Finak, G. *et al.* MAST: a flexible statistical framework for assessing transcriptional changes  
654 and characterizing heterogeneity in single-cell RNA sequencing data. *Genome Biol* **16**, 278  
655 (2015).
- 656 39. Ramesh, A. *et al.* Metagenomic next-generation sequencing of samples from pediatric  
657 febrile illness in Tororo, Uganda. *PLoS One* **14**, e0218318 (2019).
- 658 40. Kalantar, K. L. *et al.* IDseq—An open source cloud-based pipeline and analysis service for  
659 metagenomic pathogen detection and monitoring. *Gigascience* **9**, (2020).
- 660 41. Venables, W. N. & Ripley, B. D. *Modern Applied Statistics with S.* (Springer-Verlag, 2002).  
661 doi:10.1007/978-0-387-21706-2.

662

663

664

665

666 Acknowledgements: This study was performed with support from the National Institute of Allergy  
667 and Infectious Diseases-sponsored Immunophenotyping Assessment in a COVID-19 Cohort  
668 (IMPACC) Network. We gratefully appreciate support from Amy Kistler, PhD, Jack Kamm, PhD,  
669 Angela Deitweiller, PhD, Saharai Caldera, BS and Maira Phelps BS.

670

671 Funding: Funding for the COMET cohort enrollment, sample collection and data analysis derived  
672 from: K23HL138461-01A1 (CL), K24HL137013 (PGW), F32 HL151117 (AS), R35 HL140026  
673 (CSC), NIAID U19AI077439 (DJE), Chan Zuckerberg Biohub (AB, JLD). The UCSF IMPACC site  
674 was funded by NIAID U19AI077439 (DJE). Funding for enrollment of COMET participants not  
675 enrolled in IMPACC and for all sample collection and data analysis derived from K23HL138461-  
676 01A1 (CL), K24HL137013 (PGW), F32 HL151117 (AS), R35 HL140026 (CSC), and the Chan  
677 Zuckerberg Biohub (AB, JLD). Philanthropic support was provided from Mark and Carrie Casey,  
678 Julia and Kevin Hartz, Carl Kawaja and Wendy Holcombe, Eric Keisman and Linda Nevin, Martin  
679 and Leesa Romo, Three Sisters Foundation, Diana Wagner and Jerry Yang and Akiko Yamazaki.

680

681 Author contributions:

682 Conceptualization: CRL, AT, BSZ, AB, CD, SL, ER, OR, CSC

683 Methodology: CRL, AT, BSZ, AB, CD, SL, ER, OR

684 Data acquisition: RG, AJ, PHS, TJD, BSZ, AB, NJ

685 Formal analysis: AT, BSZ, AB, CD, SL, ER, EM

686 Investigation: BSZ, AB, CD, SS, CSC, DJE

687 Funding acquisition: CRL, CSC, JLD, DJE

688 Supervision: CRL, OR, NN, JLD, CSC, DJE

689 Writing - original draft: AT, BSZ, AB, CD, SL, ER, CRL

690 Writing - review & editing: All authors

691

692 Competing interests: Authors declare that they have no competing interests.

693

694 Materials and Correspondence: Correspondence and material requests should be addressed to

695 Chaz Langelier ([chaz.langelier@ucsf.edu](mailto:chaz.langelier@ucsf.edu)).

696

697 Data and materials availability: Host gene expression data are available under NCBI GEO

698 accession number GSE168019 for bulk RNA-seq and GSE168018 for scRNA-seq. Raw microbial

699 sequencing alignments are available from NCBI SRA under BioProject PRJNA704082. Code

700 used for differential expression analysis is available at <https://github.com/bspeco/VAPinCOVID19>

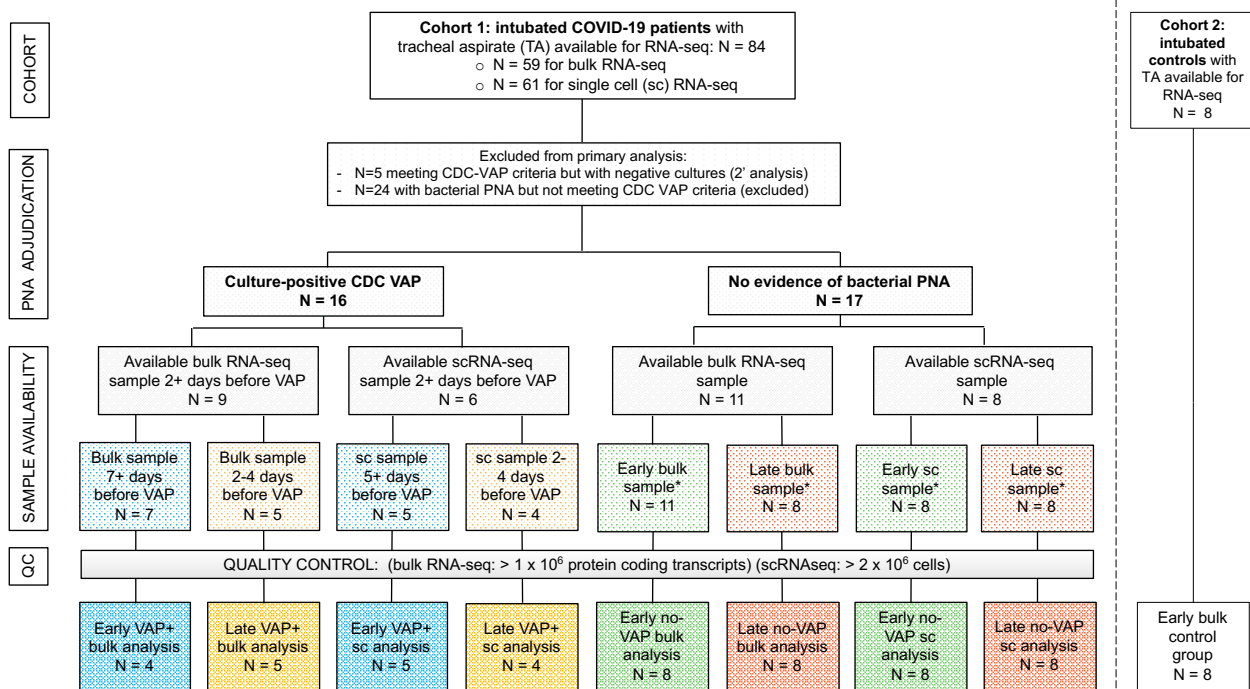


**Figure 1: Study flowchart.**

Two patient cohorts were studied. Cohort 1 consisted of COVID-19 patients from the COVID Multiphenotyping for Effective Therapies (COMET) / Immunophenotyping Assessment in a COVID-19 Cohort (IMPACC) studies (described in Methods). Cohort 2 consisted of critically ill intubated control patients from a prior prospective cohort study led by our research group<sup>18</sup>. The “early” samples were the first available tracheal aspirate specimens after intubation. For COVID-19 patients who developed VAP, the “late” samples were obtained a median of two days before VAP onset. Timing of sample collection with respect to VAP versus No-VAP groups was matched at “early” and “late” time points. Controls included eight critically ill, mechanically ventilated patients without LRTI. All COVID-19 patients included in the primary bulk analysis were also included in the longitudinal VAP host expression and microbiome analyses. Abbreviations: VAP=ventilator-associated pneumonia; TA=tracheal aspirate; QC=quality control; sc or scRNA-seq= single cell RNA sequencing; PNA=pneumonia; CDC=United States Centers for Disease Control and Prevention.

Figure 2

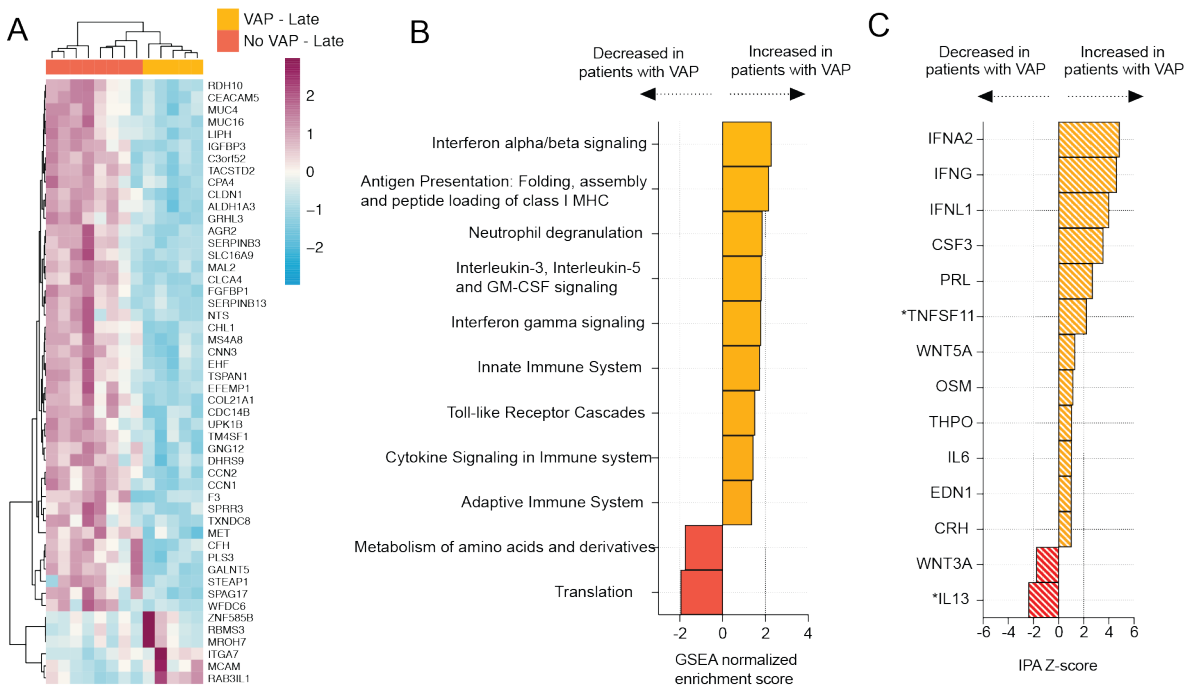


**Figure 2: COVID-19 VAP is associated with a lower respiratory tract transcriptional signature of bacterial infection 2 days before VAP onset.**

**A)** Heatmap of the top 50 differentially expressed genes by adjusted P-value between COVID-19 patients who developed VAP (yellow) versus those who did not (red) at the “late” time-point, 2 days before the onset of VAP, from bulk RNA-seq. **B)** Gene set enrichment analysis (GSEA) at the “late” time-point based on differential gene expression analyses. GSEA results were considered significant with an adjusted P-value <0.05. **C)** Ingenuity Pathway Analysis (IPA) of upstream cytokines at the “late” time-point based on differential gene expression analyses. IPA results were considered significant with a Z-score absolute value >2 and overlap P-value <0.05. \*Denotes cytokines with an overlap P-value < 0.1. All pathways and cytokines are shown in Supplementary data files 2 and 3.

Figure 3

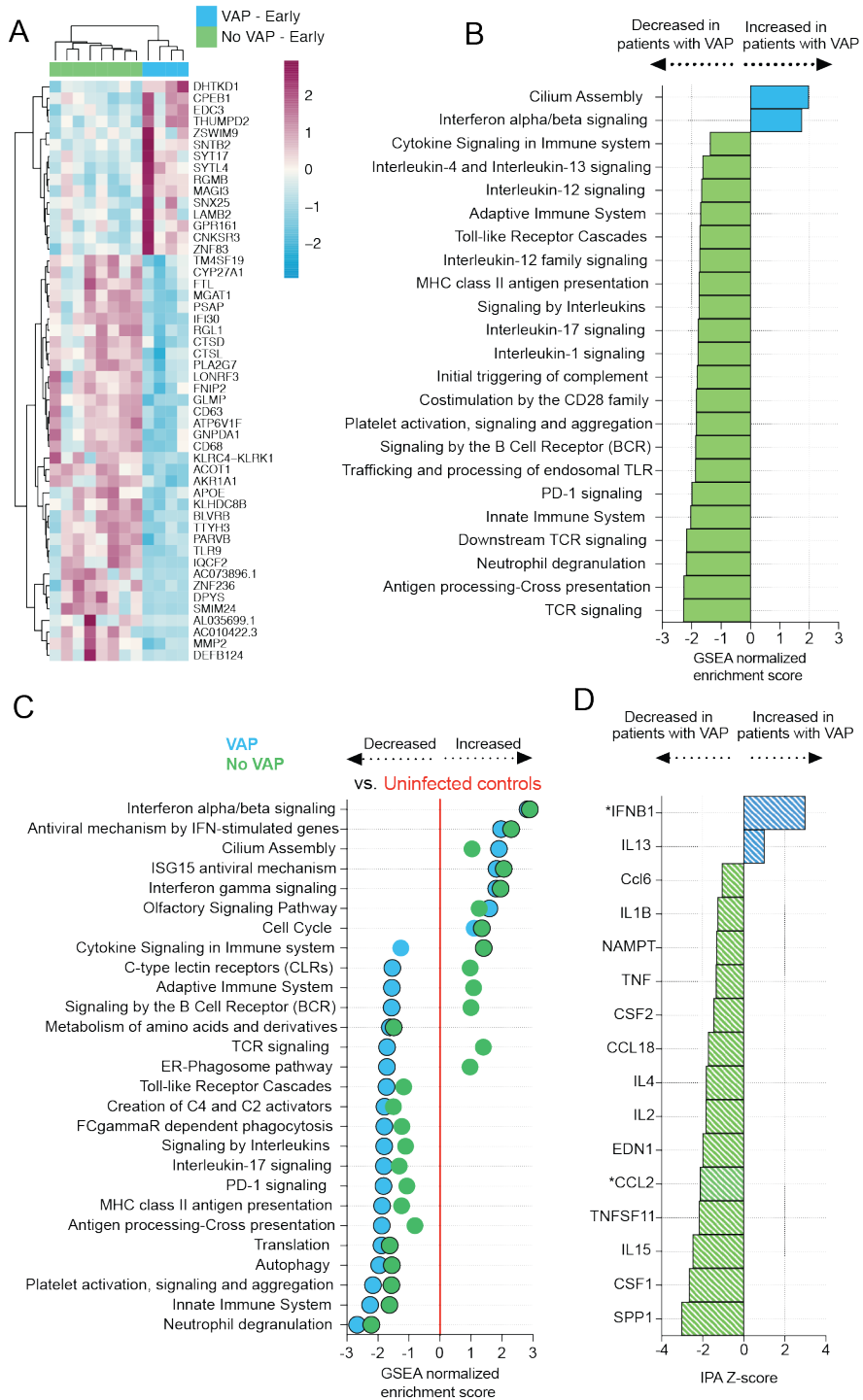




**Figure 3: COVID-19 patients who develop VAP have attenuated immune signaling in the lower respiratory tract two weeks before onset of secondary bacterial pneumonia.**

**A)** Heatmap of the top 50 differentially expressed genes by adjusted P-value between COVID-19 patients who developed VAP (blue) versus those who did not (green) at the “early” time-point from bulk RNA-seq. **B)** Gene set enrichment analysis at the “early” time-point based on differential gene expression analyses. GSEA results were considered significant with an adjusted P-value <0.05. **C)** Expression of GSEA pathways at the “early” time-point with respect to a baseline of uninfected, intubated controls. Pathways were selected from the GSEA results if they had an adjusted P-value <0.05 in at least one of the comparisons (VAP vs controls or No-VAP vs controls). Pathways with an adjusted P-value <0.05 when compared to controls are indicated by circles with a black outline. **D)** Ingenuity Pathway Analysis (IPA) of upstream cytokines at the “early” time-point based on differential gene expression analyses. IPA results were considered significant with a Z-score absolute value >2 and overlap P-value <0.05. \*Denotes cytokines with an overlap P-value <0.1. All pathways and cytokines are shown in Supplementary data files 2 and 3.

Figure 4

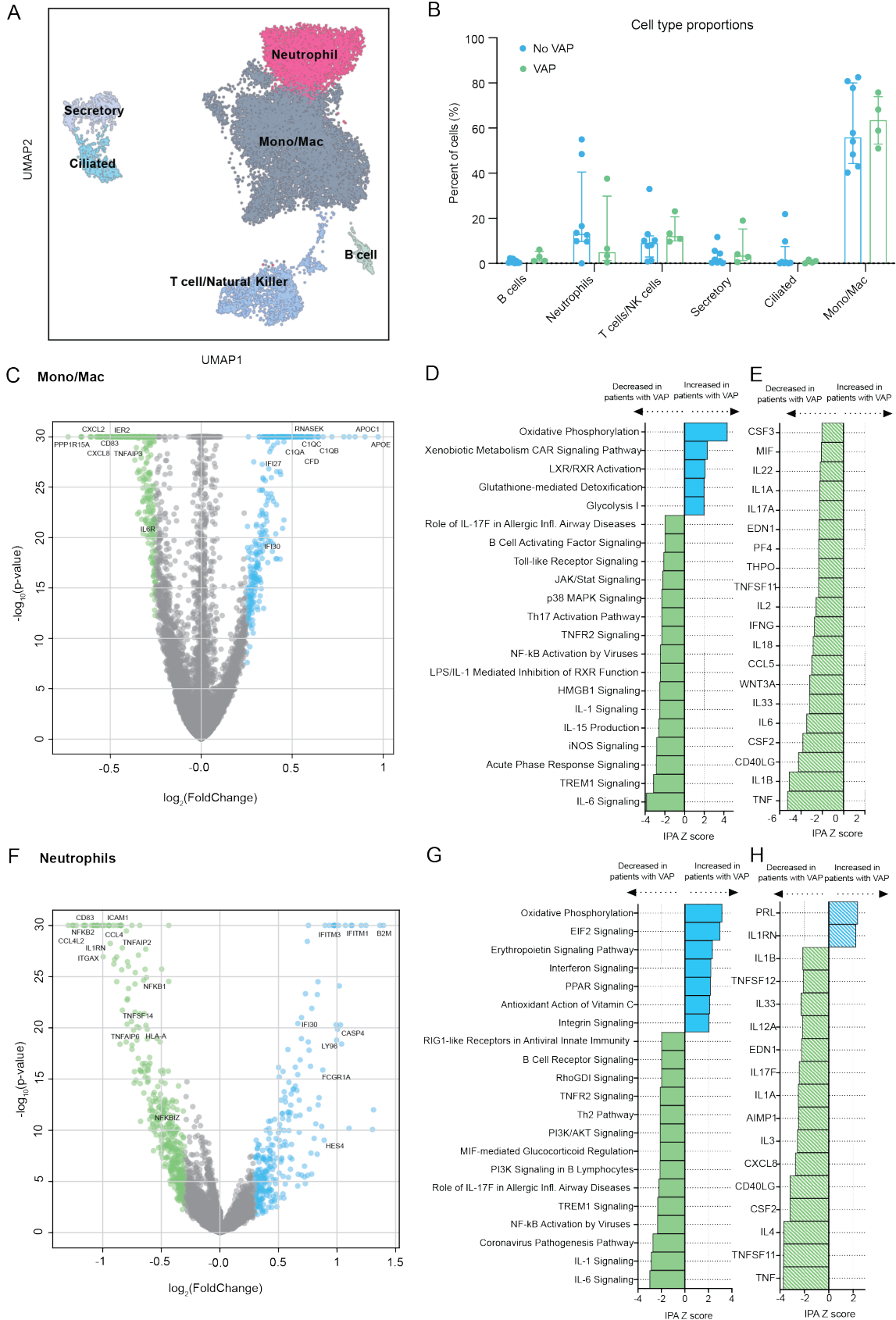


**Figure 4: scRNA-seq demonstrates that COVID-19 VAP is associated with early impaired anti-bacterial immune signaling in lower respiratory tract monocytes, macrophages and neutrophils.**

**A)** UMAP of single cell RNA-seq data from patients that do or do not develop VAP at the “early” time-point, annotated by cell type. **B)** Cell type proportions in single cell RNA-seq from VAP and No-VAP patients at the “early” time-point. Bars represent the median with IQR. Statistical significance was determined by Mann-Whitney tests. None of the cell types were significantly different with a p-value <0.05. The p-values for each cell type are as follows: B cells: 0.073; Neutrophils: 0.28; T/NK cells: 0.21; Secretory: 0.46; Ciliated: 0.94, and Mono/Mac: 0.81. **C)** Volcano plot displaying the differentially expressed genes between VAP and No-VAP patients in monocytes and macrophages. **D)** Ingenuity Pathway Analysis (IPA) of key canonical pathways and upstream cytokines based on differential gene expression analysis in monocytes and macrophages of patients who develop VAP versus those who do not, with adjusted p-values < 0.05. Only significant pathways (IPA Z-score of >2 or <-2 and overlap p-value <0.05) are shown. **E)** Volcano plot displaying the differentially expressed genes between VAP and No-VAP patients in neutrophils. **F)** IPA of canonical pathways and upstream cytokines based on differential gene expression analysis in neutrophils of patients who develop VAP versus those who do not, with adjusted p-values < 0.05. Only significant pathways (IPA Z-score of >2 or <-2 and overlap p-value <0.05) are shown. All pathways and cytokines are shown in Supplementary data files 5 and 6.

Figure 5

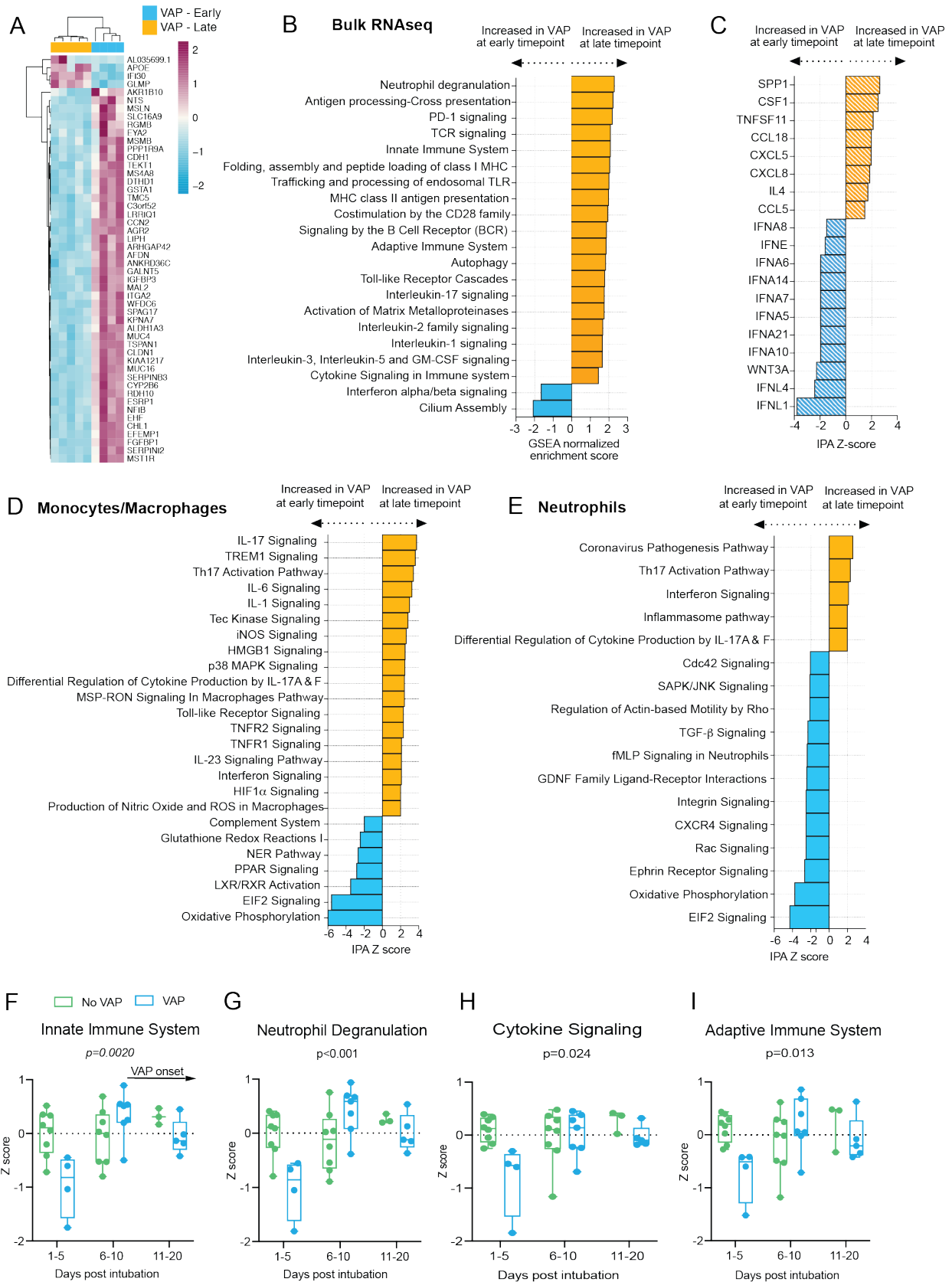


### Figure 5: Temporal dynamics of the host response to VAP

**A)** Heatmap of the top 50 differentially expressed genes by adjusted P-value between COVID-19 patients who developed VAP at the “early” time-point (blue) versus the “late” time-point (yellow) from bulk RNA-seq. **B)** Gene set enrichment analysis (GSEA) based on differential gene expression of VAP patients at the “early” vs “late” time-point from bulk RNA-seq. GSEA results were considered significant with an adjusted P-value <0.05. **C)** Ingenuity Pathway Analysis (IPA) of upstream cytokines based on differential gene expression analyses of VAP patients at the “early” vs “late” time-point from bulk RNA-seq. IPA results were considered significant with a Z-score absolute value >2 and overlap P-value <0.05. **(D-E)** Ingenuity Pathway Analysis (IPA) of key canonical pathways based on differential gene expression analysis in monocytes and macrophages (D) or neutrophils (E) from scRNA-seq of patients who develop VAP versus those who do not, with adjusted p-values < 0.05. Only significant pathways (IPA Z-score of >2 or <-2 and overlap p-value <0.05) are shown. All pathways and cytokines are shown in Supplementary data files 2, 3, 5, and 6. **(F-I)** Longitudinal analysis of selected pathway expression in VAP (blue) versus No-VAP (green) patients from bulk RNA-seq samples taken from time of intubation to onset of VAP for all patients. Pathway Z-scores were calculated by averaging Z-scores for the top 20 leading edge genes of each pathway, determined by the results of GSEA comparing VAP versus No-VAP patients at the “early” time-point. Multiple Z-scores per patient at a given time interval were averaged so that each patient corresponds to one datapoint at each interval. Samples from day 21+ after intubation are not shown due to a lack of these later time-points in the No-VAP group. VAP onset in these patients ranged from 10-39 days post intubation. Selected pathways are innate immune system (F), neutrophil degranulation (G), cytokine signaling (H), and adaptive immune system (I). Box plots represent the median and range. Statistical significance was determined by two-way ANOVA, and interaction p-values are shown.

**Figure 6**

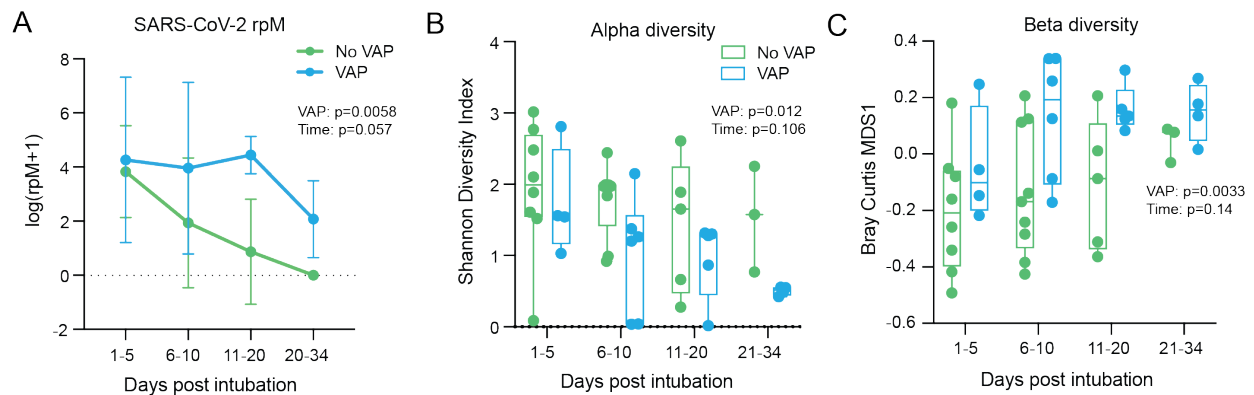


**Figure 6: Lung microbiome community collapse precedes VAP in COVID-19 patients.**

**(A)** SARS-CoV-2 viral load (reads per million sequenced, rpM) over time by days since intubation in patients who develop VAP vs those who do not. For plotting purposes,  $\log(\text{rpM}+1)$  was used to avoid negative values. Lung microbiome **(B)** bacterial diversity (Shannon's Index) and **(C)**  $\beta$ -diversity (Bray Curtis Index, NMDS scaling) in COVID-19 patients with relation to VAP development over time by days since intubation. Box plots represent the median and range (A-C). Statistical significance was determined by two-way ANOVA. P-values  $<0.05$  were considered significant.

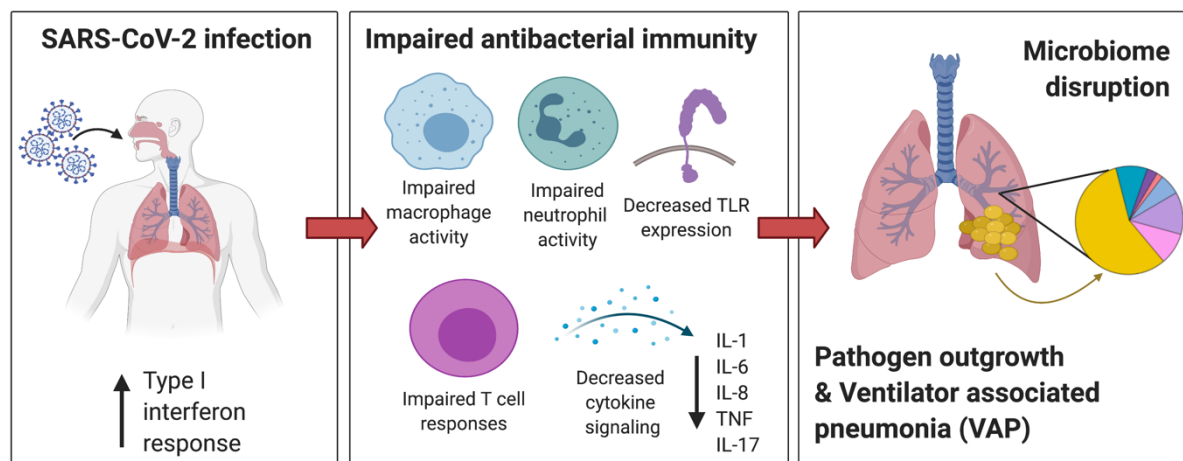


**Figure 7: Mechanistic hypothesis of secondary bacterial pneumonia susceptibility in patients with COVID-19.**

Individual immune responses to SARS-CoV-2 infection drive a restructuring of the microbial community and increase susceptibility to VAP. Those predisposed to VAP have increased type I interferon responses and dysregulated antibacterial immune signaling characterized by impaired macrophage, neutrophil and T cell activity, decreased TLR signaling and impaired activation of key cytokines important for pathogen defense including IL-1, IL-6, IL-8, TNF, and IL-17. This state of suppressed immunity disrupts the lower respiratory tract microbiome, predisposing to outgrowth of bacterial pathogens and VAP.